JGR Atmospheres

RESEARCH ARTICLE
10.1029/2024JD041720

First Time-Resolved Leader Spectra Associated With a Downward Terrestrial Gamma-Ray Flash Detected at the Telescope Array Surface Detector

Key Points:

- The first time-resolved leader spectra (400–900 nm) linked with downward Terrestrial Gamma ray Flash (TGF) were measured
- Ion optical emissions start 167 μs before detecting the downward TGF and end 267 μs after it
- Neutral optical emissions occur right at the moment of the downward TGF detection

Correspondence to:

N. Kieu,
nkieu@luc.edu

Citation:

Kieu, N., Abbasi, R. U., Saba, M. M. F., Belz, J. W., Krehbiel, P. R., Stanley, M. A., et al. (2024). First time-resolved leader spectra associated with a downward terrestrial gamma-ray flash detected at the telescope array surface detector. *Journal of Geophysical Research: Atmospheres*, *129*, e2024JD041720. https://doi.org/10.1029/2024JD041720

Received 11 JUN 2024
Accepted 25 NOV 2024

N. Kieu[1], R. U. Abbasi[1], M. M. F. Saba[2], J. W. Belz[3], P. R. Krehbiel[4], M. A. Stanley[4], F. J. Gordillo-Vazquez[5], M. Passas-Varo[5], T. Warner[6], W. Rison[4], D. Rodeheffer[4], D. R. da Silva[2], D. Mazzucco[1], T. Knight[1], I. T. Cruz[2], J. Remington[3,7], J. Mazich[1], R. LeVon[3], K. Smout[3], A. Petrizze[3], T. Abu-Zayyad[1,3], M. Allen[3], D. R. Bergman[3], I. Buckland[3], W. Campbell[3], B. G. Cheon[8], K. Endo[9], A. Fedynitch[10,11], T. Fujii[9,12], K. Fujisue[10,11], K. Fujita[10], M. Fukushima[10], G. Furlich[3], Z. Gerber[3], N. Globus[13,14], W. Hanlon[3], N. Hayashida[15], H. He[13,16], K. Hibino[15], R. Higuchi[13], D. Ikeda[15], T. Ishii[17], D. Ivanov[3], S. Jeong[18], C. C. H. Jui[3], K. Kadota[19], F. Kakimoto[15], O. Kalashev[20], K. Kasahara[21], Y. Kawachi[9], K. Kawata[10], I. Kharuk[20], E. Kido[13], H. B. Kim[8], JiHee Kim[3,22], JiHyun Kim[3], S. W. Kim[18,23], R. Kobo[9], I. Komae[9], K. Komatsu[24], K. Komori[25], C. Koyama[10], M. Kudenko[20], M. Kuroiwa[24], Y. Kusumori[25], M. Kuznetsov[20,26], Y. J. Kwon[27], K. H. Lee[8], M. J. Lee[18], B. Lubsandorzhiev[20], J. P. Lundquist[3,28], A. Matsuzawa[24], J. A. Mathews[3], J. N. Matthews[3], K. Mizuno[24], M. Mori[25], M. Murakami[25], S. Nagataki[13], M. Nakahara[9], T. Nakamura[29], T. Nakayama[24], Y. Nakayama[25], T. Nonaka[10], S. Ogio[10], H. Ohoka[10], N. Okazaki[10], M. Onishi[10], A. Oshima[30], H. Oshima[10], S. Ozawa[31], I. H. Park[18], K. Y. Park[8], M. Potts[3], M. Przybylak[32,33], M. S. Pshirkov[20,34], C. Rott[3,18], G. I. Rubtsov[20], D. Ryu[35], H. Sagawa[10], N. Sakaki[10], R. Sakamoto[25], T. Sako[10], N. Sakurai[10], S. Sakurai[9], D. Sato[24], S. Sato[25], K. Sekino[10], T. Shibata[10], J. Shikita[9], H. Shimodaira[10], B. K. Shin[35], H. S. Shin[9,12], K. Shinozaki[32], J. D. Smith[3], P. Sokolsky[3], B. T. Stokes[3], T. A. Stroman[3], Y. Takagi[25], K. Takahashi[10], M. Takeda[10], R. Takeishi[10], A. Taketa[36], M. Takita[10], Y. Tameda[25], K. Tanaka[37], M. Tanaka[38], S. B. Thomas[3], G. B. Thomson[3], P. Tinyakov[20,26], I. Tkachev[20], T. Tomida[24], S. Troitsky[20], Y. Tsunesada[9,12], S. Udo[15], F. Urban[39], I. A. Vaiman[20], M. Vrábel[32], D. Warren[13], K. Yamazaki[30], Y. Zhezher[10,20], Z. Zundel[3], and J. Zvirzdin[3]

[1]Department of Physics, Loyola University Chicago, Chicago, IL, USA, [2]National Institute for Space Research (INPE), Sao Jose dos Campos, Brazil, [3]High Energy Astrophysics Institute and Department of Physics and Astronomy, University of Utah, Salt Lake City, UT, USA, [4]Langmuir Laboratory for Atmospheric Research, New Mexico Institute of Mining and Technology, Socorro, NM, USA, [5]Instituto de Astrofisíca de Andalucía (IAA), Granada, Spain, [6]ZT Research, Rapid City, SD, USA, [7]Now at NASA Marshall Space Flight Center, Huntsville, AL, USA, [8]Department of Physics and the Research Institute of Natural Science, Hanyang University, Seoul, Korea, [9]Graduate School of Science, Osaka Metropolitan University, Osaka, Japan, [10]Institute for Cosmic Ray Research, University of Tokyo, Kashiwa, Japan, [11]Institute of Physics, Academia Sinica, Taipei City, Taiwan, [12]Nambu Yoichiro Institute of Theoretical and Experimental Physics, Osaka Metropolitan University, Osaka, Japan, [13]Astrophysical Big Bang Laboratory, RIKEN, Wako, Japan, [14]Now at KIPAC, Stanford University, Stanford, CA, USA, [15]Faculty of Engineering, Kanagawa University, Yokohama, Japan, [16]Now at Purple Mountain Observatory, Nanjing, China, [17]Interdisciplinary Graduate School of Medicine and Engineering, University of Yamanashi, Kofu, Japan, [18]Department of Physics, Sungkyunkwan University, Suwon, Korea, [19]Department of Physics, Tokyo City University, Tokyo, Japan, [20]Institute for Nuclear Research of the Russian Academy of Sciences, Moscow, Russia, [21]Faculty of Systems Engineering and Science, Shibaura Institute of Technology, Tokyo, Japan, [22]Now at Physics Department, Brookhaven National Laboratory, Upton, NY, USA, [23]Now at Korea Institute of Geoscience and Mineral Resources, Daejeon, Korea, [24]Academic Assembly School of Science and Technology Institute of Engineering, Shinshu University, Nagano, Japan, [25]Graduate School of Engineering, Osaka Electro-Communication University, Osaka, Japan, [26]Service de Physique Théorique, Université Libre de Bruxelles, Brussels, Belgium, [27]Department of Physics, Yonsei University, Seoul, Korea, [28]Center for Astrophysics and Cosmology, University of Nova Gorica, Nova Gorica, Slovenia, [29]Faculty of Science, Kochi University, Kochi, Japan, [30]College of Science and Engineering, Chubu University, Kasugai, Japan, [31]Quantum ICT Advanced Development Center, National Institute for Information and Communications Technology, Tokyo, Japan, [32]Astrophysics Division, National Centre for Nuclear Research, Warsaw, Poland, [33]Now at Doctoral School of Exact and Natural Sciences, University of Lodz, Lodz, Poland, [34]Sternberg Astronomical Institute, Moscow M.V. Lomonosov State University, Moscow, Russia, [35]Department of Physics, School of Natural Sciences, Ulsan National Institute of Science and Technology, Ulsan, Korea, [36]Earthquake Research Institute, University of Tokyo, Tokyo, Japan, [37]Graduate School of Information Sciences, Hiroshima City University, Hiroshima, Japan, [38]Institute of Particle and Nuclear Studies, KEK, Ibaraki, Japan, [39]CEICO, Institute of Physics, Czech Academy of Sciences, Prague, Czech Republic

Abstract Optical emissions associated with Terrestrial Gamma ray Flashes (TGFs) have recently become important subjects in space-based and ground-based observations as they can help us understand how TGFs are produced during thunderstorms. In this paper, we present the first time-resolved leader spectra of the optical component associated with a downward TGF. The TGF was observed by the Telescope Array Surface Detector (TASD) simultaneously with other lightning detectors, including a Lightning Mapping Array (LMA), an INTerFerometer (INTF), a Fast Antenna (FA), and a spectroscopic system. The spectroscopic system recorded leader spectra at 29,900 frames per second (33.44 μs time resolution), covering a spectral range from 400 to 900 nm, with 2.1 nm per pixel. The recordings of the leader spectra began 11.7 ms before the −18 kA return stroke and at a height of 2.37 km above the ground. These spectra reveal that optical emissions of singly ionized nitrogen and oxygen occur between 167 μs before and 267 μs after the TGF detection, while optical emissions of neutrals (H I, 656 nm; N I, 744 nm, and O I, 777 nm) occur right at the moment of the detection. The time-dependent spectra reveal differences in the optical emissions of lightning leaders with and without downward TGFs.

Plain Language Summary Spectroscopy is a powerful tool in lightning research, as it enables the identification of chemical components within the lightning channel. In this study, we present time-resolved leader spectra of the optical components associated with a downward TGF detection. The chemical makeup of these optical emissions includes nitrogen, oxygen, and hydrogen, along with measurements of their intensities and lifetimes. This marks the first time that spectroscopic optical components of lightning leaders associated with downward TGFs have been recorded. Optical emissions of ions appear before and after the detection of the TGF while optical emissions of neutrals appear at the moment of the TGF detection.

1. Introduction

Terrestrial gamma ray flashes (TGFs) are intense bursts of gamma rays with photon energies reaching several tens of MeV (J. R. Dwyer & Smith, 2005). TGFs were first detected by the Burst and Transient Source Experiment (BATSE) in 1994 (Fishman et al., 1994), and then by other satellites such as the Reuven Ramaty High Energy Solar Spectroscopic Imager (RHESSI) (Gjesteland et al., 2012; Grefenstette et al., 2009; Smith et al., 2005), the Fermi Gamma ray Burst Monitor (GBM) (M. Briggs et al., 2010; M. S. Briggs et al., 2013), the Astrorivelatore Gamma a Immagini Leggero (AGILE) satellite (Marisaldi et al., 2010a, 2010b; Tavani et al., 2011), and the Atmosphere-Space Interactions Monitor (ASIM) (Neubert et al., 2020; Østgaard et al., 2019). In addition, TGFs have also been observed by ground-based observations (J. Dwyer et al., 2004; J. Dwyer et al., 2012; Tran et al., 2015; Hare et al., 2016; Abbasi et al., 2017, 2018; Belz et al., 2020; Ortberg et al., 2020; Wada et al., 2020, 2022; Abbasi et al., 2023; Chaffin et al., 2024).

Observations showed that TGF spectra are consistent with bremsstrahlung emissions (J. R. Dwyer & Smith, 2005; Marisaldi, Fuschino, et al., 2010; Lindanger et al., 2022). The resulting gamma bursts are thought to be produced by relativistic runaway electron avalanches (RREAs), accelerated by strong electric fields inside thunderclouds (J. R. Dwyer & Smith, 2005; J. R. Dwyer, 2008; Carlson et al., 2007; Gjesteland et al., 2010; Xu et al., 2012; Marisaldi, Argan, et al., 2010; Tavani et al., 2011; Celestin et al., 2012). Calculations based on RHESSI observations show that for each TGF, the thunderstorm must have produced about 10^{16} runaway electrons for a 21 km source and about 10^{17} for a 15 km source (J. R. Dwyer & Smith, 2005). With a large number of charged particles at the source, RREAs alone are not able to explain the phenomenon. There are two possible models that could explain the mechanism: the relativistic feedback discharge (RFD) model (A. Gurevich et al., 1992; A. V. Gurevich & Zybin, 2001; L. P. Babich, 2005; J. Dwyer, 2003; J. R. Dwyer, 2005, 2007, 2012) and the lightning leader model, also known as the thermal runaway electron model (A. Gurevich et al., 2007; Carlson et al., 2009; Celestin et al., 2012; J. R. Dwyer, 2008; J. R. Dwyer & Cummer, 2013; Köhn & Ebert, 2015; Köhn et al., 2017; Köhn, Chanrion, et al., 2020; Xu et al., 2015). Although the two models are not mutually exclusive, their roles are not yet fully understood. Additional observations from ground and space-based platforms are needed to understand the mechanisms behind the TGF production better.

Since the first optical emissions associated with TGFs were detected by RHESSI and LIS (Østgaard et al., 2013), satellite observations and modeling studies have focused primarily on the timing relationship between optical emissions and TGF production (Bjørge-Engeland et al., 2022; Neubert et al., 2020; Skeie et al., 2022; Østgaard

et al., 2019; Østgaard et al., 2021). These subsequent observations show that for TGF detected from space, optical emissions associated to the TGF were always detected at the time of the TGF or after it. However, we show in the present investigation that, for downward TGFs, optical emissions associated to the TGF can also occur before it, as previously reported by Abbasi et al. (2023).

For ground-based observations of downward TGFs, the first optical emissions associated with TGFs were recently reported by Abbasi et al. (2023), based on observations at the Telescope Array Surface Detector (TASD) in west-central Utah. The optical emissions were observed to occur during Initial Breakdown Pulses (IBPs) and branching of the stepped leader of a negative-polarity cloud to ground (CG) flash during its downward development below the cloud base. The observations were based on the luminosity measurements of the scattered light from the downward leader recorded by a high-speed camera (25 μs time resolution), which constituted the sum of the intensities between 400 and 1,050 nm.

To enhance our understanding of the atomic and molecular components involved in the optical observations, we installed a spectroscopic measurement system at the TASD site. The setup enables us to observe the optical components of leaders associated with TGFs on a time-resolved basis. The spectroscopic system records the optical signals at different spectral lines, facilitating the identification of the chemical components within the optical emissions from the leaders. By correlating the leader spectra with TGF detections from the TASD, we aim to delineate the chemical composition of the lightning flash stages that are conducive to TGF production from those that are not.

Unlike return strokes, the leader phase of a lightning flash is characterized by a range of weakly luminous events, posing challenges for their observations. Consequently, there have been relatively few reported observations of the leader spectra. Most of these observations were recorded just a few hundred microseconds before the return strokes and a few hundred meters above the ground. The first stepped-leader spectrum was recorded on film from 560 to 660 nm by Orville (1968). Several years later, Orville (1975) reported spectra of five dart leaders from 398 to 510 nm. Thanks to the development of new digital high-speed cameras, leader spectra have been observed for more events and over wider spectral ranges. Warner et al. (2011) recorded five stepped leader spectra from 600 to 1,050 nm at 10,000 frames per second. Cen et al. (2015) presented spectra of five dart leaders observed from 400 to 900 nm at 9,110 frames per second. Recently, Harley et al. (2021) reported on spectra of a bolt from the blue (BFB) lightning stepped leader in the spectral range from 400 to 900 nm. At the time of writing this work, no observations were reported on the spectroscopy of the initial leader stages of lightning in correlation with the initial breakdown pulses stage.

In this work, we present the first time-resolved leader spectra of the optical components in association with downward TGF detection. The spectra were observed from 400 to 900 nm, with time resolutions of 33.44 μs recorded during the initial breakdown pulse stage of lighting. These spectra show that the optical emissions can occur before the downward TGF occurs. After the introduction (Section 1), this study is structured into three additional sections. Section 2 explains the experimental setup and includes a brief introduction to all instruments involved in the observation. Section 3 shows the TGF observations by the TASD and other lightning detectors at the TASD site. Finally, Section 4 focuses on the spectral analysis of the return strokes and leaders associated with the TGF detection.

2. Experimental Setup

The experiment was conducted at the Telescope Array Surface Detectors (TASDs) site. The TASDs recorded the TGF waveform, while other lightning detectors captured lightning information from the flash that produced the TGF. The spectroscopic system was housed in the same building as other lightning detectors, including a Lightning Mapping Array (LMA), an Interferometer (INTF), and a Fast Antenna (FA). Below are brief introductions to these instruments; more details can be found in Abu-Zayyad et al. (2012); Abbasi et al. (2017, 2018); Belz et al. (2020); Abbasi et al. (2023).

The TASD is a ground-based telescope observatory located in the desert west of Delta, Utah. It consists of 507 Scintillator Detectors (SDs), each with an area of 3 m^2 and 1.2 km away from each other, covering an area of 700 km^2. The TASD was primarily designed to detect the Extensive Air Shower (EAS) charged components with a sampling rate of 20 ns. The TASD gets triggered when three adjacent SDs observe a signal greater than 3 Minimum

Ionizing Particles within 8 μs (~150 FADC counts). When a trigger event occurs, the signals from all individually triggered SDs within ±32 μs are recorded. More details of the TASDs can be found in Abu-Zayyad et al. (2012).

The Lightning Mapping Array (LMA) consisted of 11 stations deployed across the 700 km^2 area, covering the TASD site. Developed by the Langmuir Laboratory group at New Mexico Tech (Rison et al., 1999; Thomas et al., 2004), the LMA determines three-dimensional locations of impulsive VHF radiation events in successive 80 μs time intervals. For the present study, the LMA observations were used to determine the plan distance to the TGF events.

The INTerFerometer (INTF) was installed in 2018, 5 km to the east of the TASD site. The INTF records broadband (20–80 MHz) waveforms at 180 MHz from three flat-plate receiving antennas. The INTF data was used to determine the two-dimensional azimuth and elevation arrival directions of the VHF radiation with sub-microsecond resolution (Stock et al., 2014).

The Fast electric field change Antenna (FA) provided high resolution (180 MHz) measurements of the low-frequency discharge sferics, which are crucial to interpreting the INTF and LMA observations (Belz et al., 2020; Liu et al., 2019).

The spectroscopic system was installed in 2022, housed in the same building as the INTF system host PC. It consists of a grism (diffraction grating plus prism, 600 lines/mm) placed in front of a high-speed camera mounted with a 14 mm lens (F/2.8). The high-speed camera is a monochrome Phantom v711 operating at 29,900 frames per second (33.44 μs time resolution) with an exposure time of 14.9 μs. The spectra images were recorded on a sensor size of 880 × 227 pixels, covering a spectral range from 400 to 900 nm. The camera's field of view (84°) covered most of the TASD's area. The system was triggered automatically by changes in luminosity detected by the camera.

3. TGF Observation at the TASD Site

On 10 August 2022, a TGF was detected at the westernmost part of the Telescope Array Surface Detectors (TASD) at 23:53:59.182,259 UTC. The TGF was produced by the initial downward leader of a negative cloud-to-ground flash, whose ensuing return stroke had a peak current of −18 kA, as determined by the National Lightning Detection Network (NLDN). Data collected from NLDN, LMA, TASD, and INTF instruments have shown that the TGF source altitude was 2.37 km above the ground and 32.3 km away from the high-speed camera, as shown in the left panel of Figure 1.

The right panel of Figure 1 shows the footprint of the TGF at the different TASD stations, indicating their energy deposit and arrival times. Numbers on each circle indicate the energy deposit in Vertical Equivalent Muons (VEMs), where each VEM equals 2.04 MeV, and circle sizes are proportional to the energy deposit in the log scale. The TASD recorded a total energy deposit of 150 MeV for the TGF. The two-dimensional velocity of the radio sources observed by the INTF and associated with the TGF observation was found to be 5.0×10^7 m/s. This was calculated based on a linear fit of elevation versus time, as previously discussed in (Abbasi et al., 2023; Belz et al., 2020). Details of the observations from various detectors are summarized in Table 1.

Figure 2 shows the signal waveforms of the TGF observed in conjunction with time-matching data from the Fast Antenna (FA) and the Interferometer (INTF). Note that the TGF detected time plotted in the figure differs from the detected time indicated in Table 1 due to the distance between the TASD detectors and the INTF/FA/Camera location, as illustrated in Figure 1. A time shift of 98 μs, utilizing the iteration procedure described in Belz et al. (2020), was added to the TASD observed time to match it with the time detected by the INTF, FA, and camera.

The upper panel of Figure 2 shows 15 ms of observations from the start of the lightning flash to the return stroke and a zoomed-in view of a 0.28 ms interval centered around the TGF detection time. The TGF waveform observations are colored according to their arrival times, as shown Figure 1. The TGF was observed during the initial breakdown pulse, as seen in the FA waveform and was accompanied by fast ($\sim 5 \times 10^7$ m/s) downward development of the VHF sources in the INTF data. The results are consistent with previous observations at the TASD (Abbasi et al., 2017, 2018, 2023; Belz et al., 2020) that TGFs are produced in association with the Initial Breakdown Pulses (IBPs) during the downward-developing leader phase.

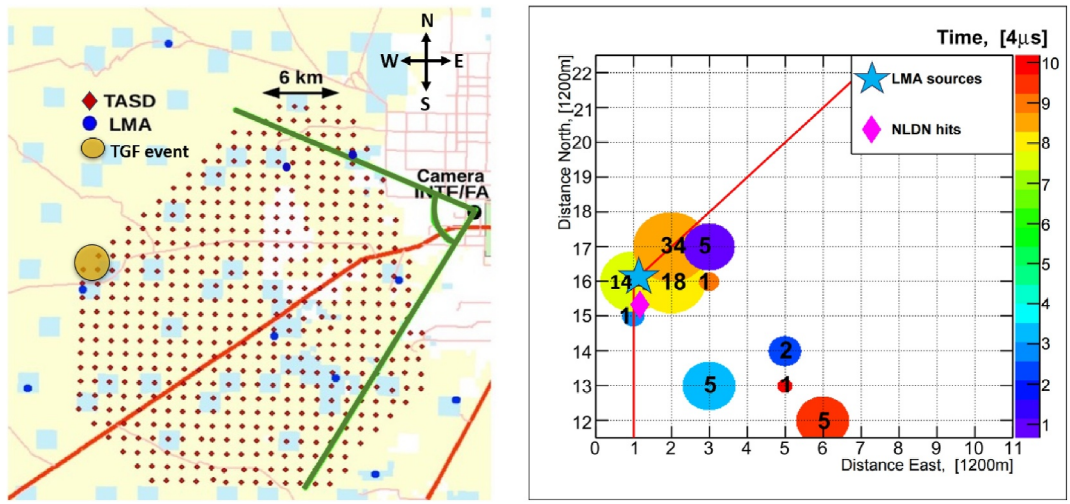

Figure 1. Locations of the detected TGFs and associated instruments. The left panel represents the TASD territory with 507 TASD stations, marked by red diamonds, covering an area of 700 km^2. The high-speed camera, INTF, and FA are all located at the same site to the east of the TASD. The field of view of the camera is limited by the two green lines forming an angle of 84°. The detected TGF is highlighted with a yellow circle at the edge of the TASD site. Blue circles denote 11 LMA sensors. The right panel illustrates the TGF footprint on the TASD. Circle sizes are proportional to the log-scale energy deposit, and colors indicates timing in 4 μs steps relative to the event trigger. Numbers on each detector displayed the energy deposit in Vertical Equivalent Muons (VEMs), where each VEM is equivalent to 2.04 MeV. The blue star denotes the LMA source, while the magenta diamond represents NLDN data locations.

Finally, it should be noted that the TGF was detected at the very northwestern edge of the TASD and that the LMA sources during the first few milliseconds of the flash were located about a kilometer or so southwest of the TASD's corner area where the detections were clustered. However, the NLDN shows that the ensuing return stroke occurred almost precisely at the corner of the cluster (blue star in the footprint of Figure 1). This suggests that additional gamma ray emissions may occur outside the TASD, either associated with earlier phases of the leader or with this gamma ray observation, indicating that our current observations represent only a lower limit of the footprint/energy deposited by the TGF observed.

4. Spectroscopic Data Analysis

The spectroscopic system was housed at the TASD site, facing the TASD area. The camera's field of view is limited by the two green lines, as shown in Figure 1. The system consists of a grism placed in front of a high-speed camera mounted with a 14 mm lens. This system is known as a slitless spectrograph.

For a slitless spectrograph, the wavelength identification and the spectral resolution vary and depend heavily on the location of the lightning channel. Therefore, to enhance the accuracy of the data processing, we first processed

Table 1
Quantitative Values of the LMA, NLDN, and TASD Observations of the Lightning Flash Producing TGF During Its Initial 1–2 ms

Date	Time	μsec	LMA dBW	NLDN I_{pk}	TASD energy sum VEM/MeV	Number of TASD's	Velocity m/s	Height Km
2022/08/10	23:53:59	182,096		−13 kA/IC				
		206		−7 kA/IC				
		249	18.8					
		257		4 kA/IC				
		259			73/150	6	5.0×10^7	2.37
		193,600		−18 kA/CG				

Note. The detected time of the LMA, NLDN, and TASD events are shown in chronological order. The LMA sensor recorded the VHF source powers. The NLND detected the peak currents (I_{pk}) and classified them as intra cloud (IC) or cloud-to-ground (CG) flash. The TASD measured the total energy deposited in all adjacent surface detectors. The last three columns are the number of TASDs contributing to the total energy, the 2-dimensional velocity, and source altitude.

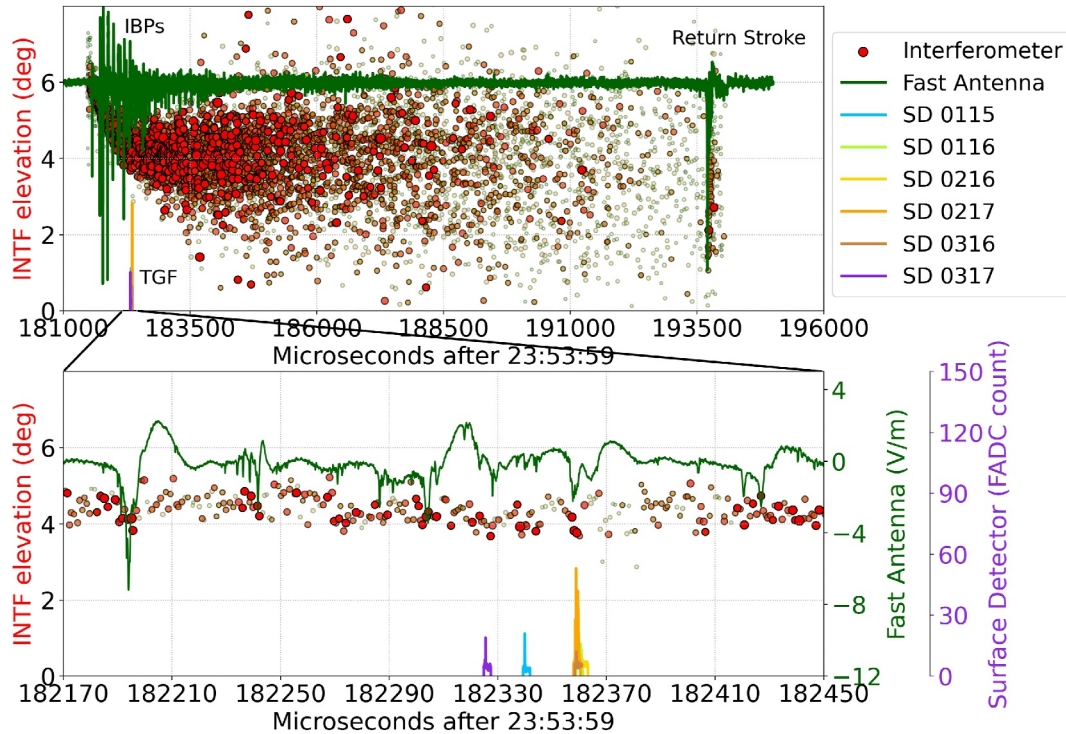

Figure 2. TGF signal waveforms recorded by different Scintillation Detectors (SD) are plotted in conjunction with data from the Fast Antenna (FA) and the Interferometer (INTF). The waveform colors correspond to the arrival time colors as shown in Figure 1. Red dots represent INTF data, with their sizes and colors proportional to the power of the radio signal, and those with lighter or non-red colors indicate data with low radio signals. Green line signals depict the changing electric field recorded by the FA. The upper panel shows the recording from the initiation of the flash until the first return stroke within 15 ms, while the lower panel provides a zoomed-in view of the upper panel within 0.28 ms.

the return stroke images due to their stronger intensity compared to the leader images, then, we applied the same process to the leader images.

In this section, we present the time-resolved spectra of the return stroke and leaders of the lightning flash associated with the TGF. The section is divided into two parts: the first part focuses on the time-resolved spectra of the return stroke, which aids in wavelength identification. The second part examines the optical emissions from leader spectra related to TGF production, followed by a discussion of the spectroscopic results in the context of detecting downward TGFs.

4.1. Time-Resolved Spectra of Return Stroke

The time-resolved spectra of the −18 kA cloud-to-ground return stroke were analyzed by the first order of spectral images captured by the high-speed camera. The raw images are shown in the left panel of Figure 3. These images display a sequence of the first five frames (167 μs in total) of the return stroke, including the zero and first-order of the dispersion. The dispersion was caused when a white light beam passes through a grism (a combination of a prism and a diffraction grating), creating interference of different wavelengths. This results in a central maximum (zero order) and other rainbow orders, such as the first, second, third order, etc.

We began by cropping the spectral images near the flash tip of the first order of the dispersion, as illustrated by the white-border rectangles in Figure 3. The white rectangle regions 230 × four pixels are the same for the five return stroke images. We then summed over four rows of this area to enhance the signal-to-noise ratio of the uncalibrated spectral. To flatten these spectra, we applied a polynomial fit to the image background and subtracted it. We assigned wavelength values by identifying strong emission lines according to well-known lightning spectra shown in previous works (Warner et al., 2011; Walker & Christian, 2017, 2019; N. Kieu et al., 2021). Finally, we followed the National Institute of Standards and Technology (NIST) Atomic Spectra Database (Kramida et al., 2012) to identify others.

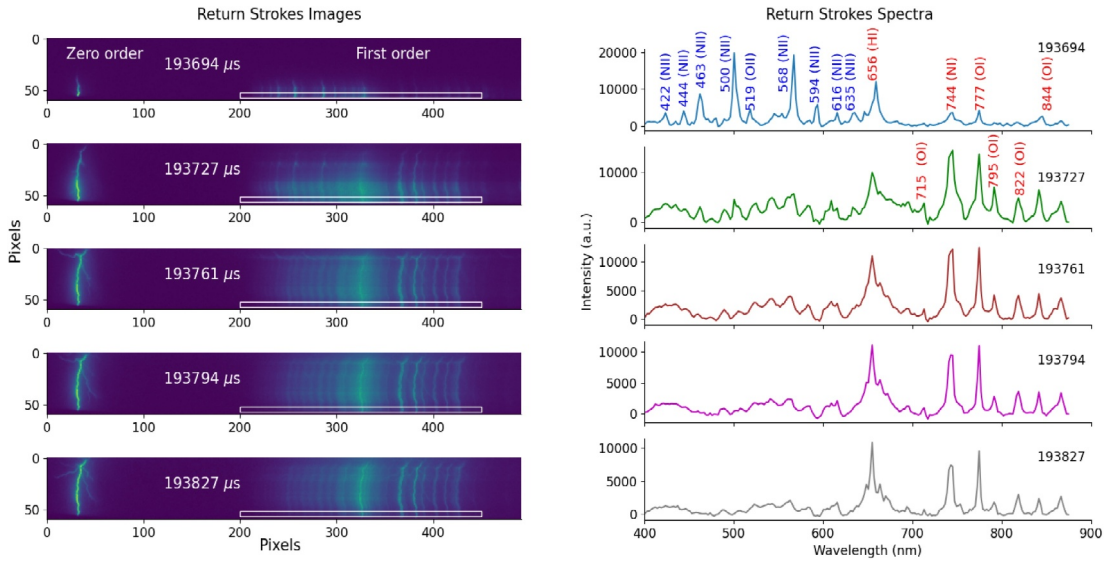

Figure 3. Time-resolved spectra of the return stroke that produced the TGF. The left panel shows a sequence of the first five images of the return stroke, and white rectangles represent the trimmed areas from which we extracted the time-resolved spectra. The right panel displays the time-resolved return stroke spectra chronologically from top to bottom. Spectra at different times are shown in different colors. Optical emissions are labeled with their wavelength numbers in nanometers and their atomic ionization states. Blue colors indicate ion emissions and red colors show neutral emissions. Note that, from the second image, the oxygen-neutral lines 715 nm, 795 nm, and 822 nm start to be visible.

The resulting time-resolved spectra of the return stroke are displayed sequentially from top to bottom, as shown in the right panel of Figure 3. The first spectrum is dominated by singly ionized nitrogen lines at 422 nm, 444 nm, 463 nm, 500 nm, 568 nm, 594 nm, 616 nm, 635 nm, and a singly ionized oxygen line at 519 nm, as shown in blue colors. Neutral emissions of hydrogen (656 nm), nitrogen (744 nm), and oxygen (777 and 844 nm), as shown in red colors, are also present but exhibit lower intensity, except the neutral hydrogen, H I at 656 nm. Please note that the emission intensity at 656 nm could be caused by the overlapping of two singly ionized nitrogen lines, N II at 648 and 661 nm, due to the limitations of our spectral resolutions (2.1 nm per pixel). These two emissions are well-known in the spectra of the return stroke.

From the second spectrum onward, spectral lines of singly ionized species disappear while optical emissions from some neutral species become significantly more prominent, O I lines at 744 nm, 777 nm, and 844 nm, and additional (but relatively weak) neutral oxygen lines at 715 nm, 795 nm, and 822 nm emerge. In fact, all these neutral lines last up to hundreds of microseconds. The presence of ion lines in lightning spectra indicated larger electron/gas temperature in the lightning channel (N. Kieu et al., 2020), from which we can consider that the temperature/energy decreases from the second frame in Figure 3.

The presence of ion and neutral lines in the recorded spectra can provide a rough estimation of the electron/gas temperature of the hot plasma channel of the return strokes and leaders. In general, more energy is required to produce and excite ions than to produce and excite neutrals from air molecules (N_2, O_2, H_2). For example, the production (starting from N_2) of singly ionized nitrogen N II emitting at 500 nm requires ~47 eV (for the dissociation of N_2 into N I atoms, ionization of N I into ground state N II ions, and, finally, for the excitation of N II). Similarly, an amount of ~21 eV is needed to produce (starting from N_2) excited N II ions emitting at 568 nm. On the other hand, the production of neutral lines requires less energy. For instance, the production (starting from H_2) of excited hydrogen atoms H I emitting the H_α line (656 nm) requires ~17 eV, and the production (starting from O_2) of excited neutral oxygen atoms O I emitting the triplet 777.4 nm requires ~16 eV. Typical experimental values of the measured electron/gas temperatures (mean electron/gas energies) from return strokes and leaders range between about 1.5 eV and a maximum of 3.5 eV, corresponding to 17,000 K to 40,000 K (1 eV is equivalent to 11,600 K). For example, the temperature in the hot channel of a 17.4 kA triggered return stroke reached 42,000 K (3.6 eV), and their optical spectra showed that the highest temperature (42,000 K) was achieved while ions were present in the spectra, that is, at the onset of the return stroke (Walker & Christian, 2019). Similar results

(ions presence when largest temperatures are measured) were found in experiments with laboratory lightning-like discharges (N. Kieu et al., 2021).

Since we were not able to calibrate our slitless spectrograph (calibration means correcting the system's response to different wavelengths), we could not use the ion and/or neutral spectral lines to calculate the electron/gas temperatures associated with the spectra of the return stroke or the leader. However, the right panel of Figure 3 shows several singly ionized emissions in the first frame, and then these ion emissions died out while neutral emissions started to grow from the second frame and lasted up to 400 μs. This behavior means that at the beginning of the return stroke, the plasma channel was in a hot and energetic period, and then it began to cool down gradually. These observations are similar to what had been reported by triggered lightning (Walker & Christian, 2019) and by laboratory lightning-like discharges (N. Kieu et al., 2021).

4.2. Time-Resolved Spectra of Leaders Associated With TGF Production

This section focuses on the time-resolved spectra of the cloud-to-ground leader associated with the observed TGF. The spectra images were captured by the same slitless spectrograph, which captured the return stroke spectra but 11.7 ms earlier. The analysis process is similar to the process described in the spectra of the return stroke, except for the trimmed areas (the white rectangles) due to the difference in the altitude of the return stroke and the leader channel.

Figure 4 displays the high-speed camera leader images and their corresponding time-resolved spectra sequentially from top to bottom. Based on the chemical components produced during the optical emissions, these leader spectra were classified into three types: "ion emissions" spectra, "neutral emissions" spectra, and "no emissions" spectra, as described below.

- "Ion emissions", indicated by the blue triangles, are the spectra displaying optical emissions dominated by singly ionized nitrogen (463 nm, 500 nm, 568 nm), oxygen (519 nm), neutral nitrogen (744 nm), oxygen (777 nm), and hydrogen (656 nm). They are frames recorded at 182,190 μs (~133 μs before TGF first detection at 182,323 μs), 182,290 μs (~33 μs before TGF first detection at 182,323 μs), and 182,424 μs (~67 μs after TGF detection at 182,357 μs).
- "Neutral emissions", indicated by the red squares, are the spectra displaying optical emissions dominated by neutral nitrogen (744 nm), oxygen (777 nm), and hydrogen (656 nm). They are frames recorded at 182,323 μs (during TGF) and 182,357 μs (during TGF).
- "No emissions", indicated by the gray circles, are the spectra with no dominating optical emissions from any atoms or ions. They are frames recorded at 182,223 μs (~100 μs before TGF detection), 182,257 μs (~66 μs before TGF detection), and 182,390 μs (~33 μs after TGF detection).

These "ion", "neutral", and "no" optical emissions were recorded in a period of 1.67 ms around the detection of the downward TGF, 0.27 ms before and 1.40 ms after it as shown in Figure 5. Interestingly, the period around the TGF detection (~437 μs, see Figure 5) is dominated by ionic optical emissions, but right at the moment when the TGF was detected (at 182,323 μs and 182,357 μs), only neutral emissions were recorded. The presence of neutral emissions at the moment of TGF detection suggests that the optical emissions occurring before and after the TGF are more energetic (they come from the deexcitation of ionic species) than optical emissions produced right when the TGF is detected.

While the spectra of the return stroke (Figure 3) look "normal", the leader spectra are not. By "normal" we mean that ions in the spectra only appear at the onset (first spectrum at 193,694 μs) of the return stroke corresponding with the moment when the largest temperature is achieved (N. Kieu et al., 2020; Walker & Christian, 2019). However, the leader spectra (Figure 4) are unusual since ion lines appear and reappear. Ion emissions first appear in the leader spectrum at 182,190 μs; then, no ion or neutral lines were recorded in the following two spectra. Suddenly, in the leader spectrum at 182,290 μs, ion emission lines reappear just before the production of the downward TGF. The reappearance (emergence) of ion spectral lines could be explained by the presence of residual ions, which is a part of the preionization left behind by the corona streamers in the tip of the leader (L. Babich et al., 2015; Köhn, Chanrion, et al., 2020).

The high temperature at the onset of a return stroke and/or a leader channel dissipate in about 10 μs (for instance, from 40000 to 20,000 K in a 17.4 kA triggered return stroke as reported by Walker and Christian (2019)). Usually, temperatures after about 10 μs can no longer be measured using ion lines since they have almost completely

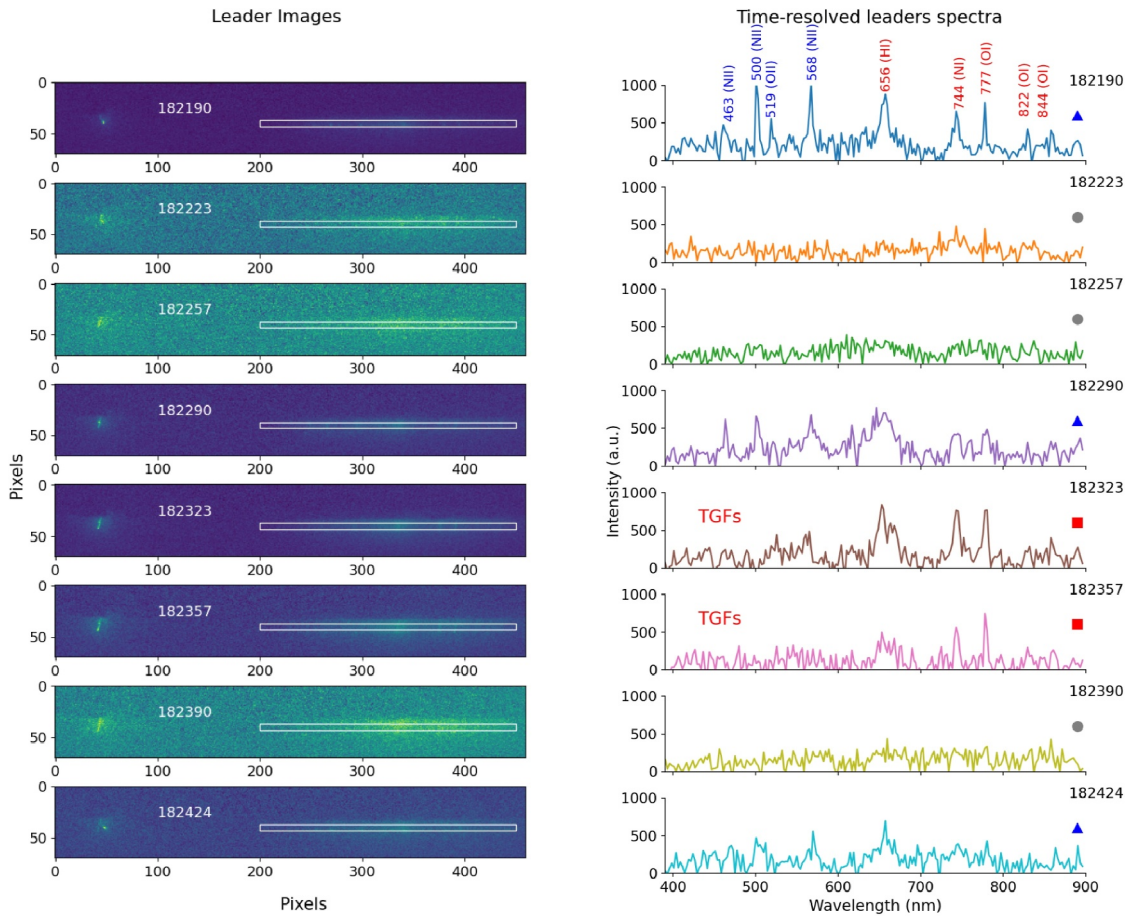

Figure 4. The first time-resolved spectra of leaders associated with TGF production. The left panel displays eight spectral images closest to the TGF detected time in chronological order from top to bottom. White rectangles represent the trimmed areas from which we extracted the time-resolved leader spectra. The right panel shows the corresponding spectra to images in the left panel. Spectra at different times are shown in different colors. Optical emissions are labeled with their wavelength numbers [nanometer] and with colors: blue indicates ion emissions, and red indicates neutral emissions. Symbols on the right side of the right panel show our spectra classification: "blue triangles" represent leader spectra with ion emissions, "red squares" represent leader spectra with neutral emissions, and "gray circles" represent leader spectra with no emissions.

disappeared from the spectra. Thus, the presence of ions in a period of ∼434 μs is not expected and has not been observed to the best of our knowledge in a moment of the dynamics of the return stroke or the leader hot plasma channel away from their onset times or very close (≤10 μs) to it. Significant concentrations of ground state ions can still exist at temperatures below 15,000 K (measurable limit through optical spectra) (see supplementary material in N. Kieu et al. (2020)) but, in the thermal environment (gas and electron temperatures are the same) of a hot leader tens of microseconds after its onset, ions are not excited by collisions with electrons or heavy species (atomic or molecular species) any longer because their mean energies are not sufficiently high (15,000 K or lower). However, if there is a certain level of preionization in the air surrounding the leader tip, it can lead to a sufficiently high production rate of runaway electrons with energies capable of exciting previously de-excited ions in the hot leader channel, leading to the initiation of the observed TGFs in this work (L. Babich et al., 2015; Köhn, Chanrion, et al., 2020).

The observations of ionic spectral lines around the downward TGF detection during the initial breakdown pulses in this study could be explained by the preionization left behind by the corona streamers and the air perturbation in front of the leader tip, which leads to a suggestion that the production of downward TGFs is related to the streamer-leader process of cloud-to-ground lightning. Interestingly, Köhn, Heumesser et al. (2020) interpretation of ASIM observations also suggests that the production of TGFs is related to the streamer coronae activity of intracloud lightning.

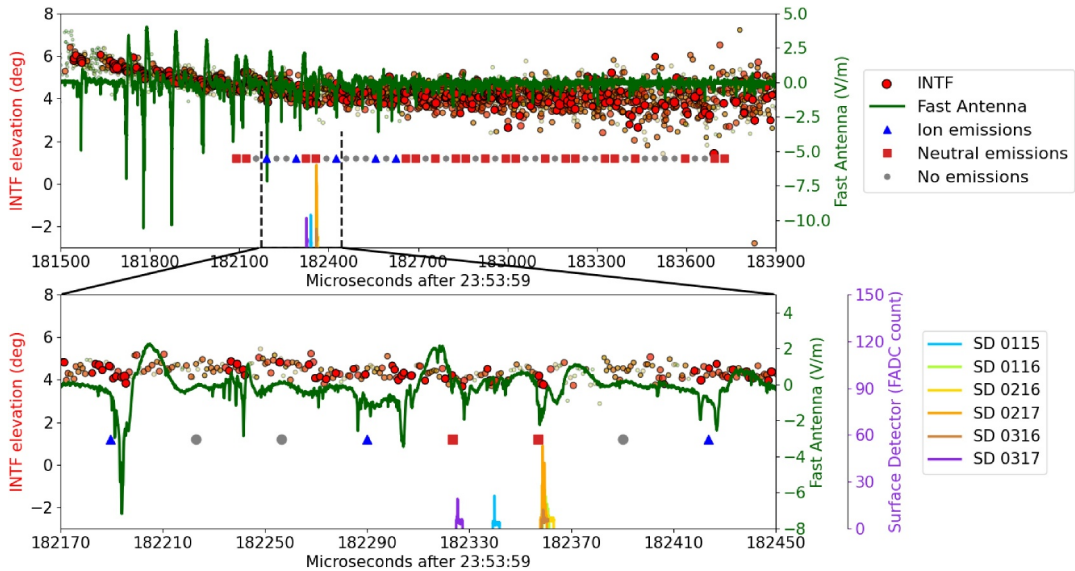

Figure 5. Optical emissions recorded by the spectroscopic system were plotted in conjunction with TGF waveforms recorded by the TASD, the FA signals, and the INTF data. The waveform colors correspond to their arrival time colors in Figure 1. Red dots represent INTF data, with their sizes and colors proportional to the power of the radio signal, and those with lighter or non-red colors indicate data with low radio signals. Green lines depict the changing of the electric field recorded by the FA. The upper panel shows the observation over a period of 2.4 ms from the initial of the lightning flash, while the lower panel is a zoom of the top panel in the interval of 0.28 ms between the two dash lines. Eight spectra between the two dashed lines are the closest to the TGF detection, shown in Figure 4. The *y*-axis of the FA scale on the right side indicates the correspondence between the magnitude of the FA signals and the observations of "ion emissions," "neutral emissions," and "no emissions" spectra.

5. Summary and Conclusions

In this work, we present the first time-resolved optical spectra of lightning leader associated with a downward TGF production. The TGF was recorded by the Telescope Array Surface Detector (TASD) during the initial breakdown pulse (IBP) stage of a lightning flash. The leader spectra were captured by a slitless spectrograph with a time resolution of 33.44 μs and a spectral resolution of 2.1 nm per pixel, covering the spectral range from 400 to 900 nm.

The optical emissions in the leader spectra were observed at 0.27 ms before and 1.40 ms after the downward TGF detection. Ionic optical emissions mostly dominate in the period directly around TGF detection (∼434 μs), but right at the moment when the TGF was detected, neutral optical emissions dominate. This suggests that the optical emissions occurring before and after the TGF are more energetic than those produced when the TGF is detected.

Moreover, the presence of the ionic emission in a period greater than a few hundred microseconds (∼437 μs) is unexpected and has not been observed to the best of our knowledge. The presence and reappearance of ions before and after TGF detection could be caused by the preionization left behind by corona streamers. As a result, the preionization and air perturbation at a certain level around streamer accelerations can lead to a high production rate of runaway electrons and ions that are spectroscopically observed around the occurrence of the downward TGF. The observations of ionic spectral lines around the TGF detection suggest that the production of downward TGF is related to the streamer-leader process of cloud-to-ground lightning.

Optical emissions from lightning leaders associated with TGF production have previously been observed from space (Bjørge-Engeland et al., 2022; Heumesser et al., 2021; Köhn et al., 2024; Neubert et al., 2020; Skeie et al., 2022; Østgaard et al., 2019, 2021) and by a ground-based detector (Abbasi et al., 2023). Contrarily to ASIM observations of optical emissions associated to TGF only occurring at the onset of the TGF or after it (Skeie et al., 2022), we report here optical emissions occurring before, during and after the downward TGF occurs, with the particularity that ion spectral lines appear not only at the onset of the leader but also just before the downward TGF is detected.

Acknowledgments
Operation and analyses of this study have been supported by NSF grants AGS-2112709, AGS-1844306, AGS-1613260, AGS-1205727, AGS-1720600, and AGS-2214044. The support by Fundação de Amparo à Pesquisa do Estado de São Paulo —FAPESP (projects 2022/10808-4 and 2023/03908-5). The Telescope Array experiment is supported by the Japan Society for the Promotion of Science (JSPS) through Grants-in-Aid for Priority Area 431, for Specially Promoted Research JP21000002, for Scientific Research (S) JP19104006, for Specially Promoted Research JP15H05693, for Scientific Research (S) JP19H05607, for Scientific Research (S) JP15H05741, for Science Research (A) JP18H03705, for Young Scientists (A) JPH26707011, and for Fostering Joint International Research (B) JP19KK0074, by the joint research program of the Institute for Cosmic Ray Research (ICRR), The University of Tokyo; by the Pioneering Program of RIKEN for the Evolution of Matter in the Universe (r-EMU); by the U.S. National Science Foundation awards PHY-1806797, PHY-2012934, PHY-2112904, PHY-2209583, PHY-2209584, and PHY-2310163, as well as AGS-1613260, AGS-1844306, and AGS-2112709; by the National Research Foundation of Korea (2017K1A4A3015188, 2020R1A2C1008230, and 2020R1A2C2102800); by the Ministry of Science and Higher Education of the Russian Federation under the contract 075-15-2024-541, IISN project No. 4.4501.18, by the Belgian Science Policy under IUAP VII/37 (ULB), by National Science Centre in Poland Grant 2020/37/B/ST9/01821, by the European Union and Czech Ministry of Education, Youth and Sports through the FORTE project No. CZ.02.01.01/00/22_008/0004632, and by the Simons Foundation (00001470, NG). This work was partially supported by the grants of the joint research program of the Institute for Space-Earth Environmental Research, Nagoya University and Inter-University Research Program of the Institute for Cosmic Ray Research of University of Tokyo. The foundations of Dr. Ezekiel R. and Edna Wattis Dumke, Willard L. Eccles, and George S. and Dolores Doré Eccles all helped with generous donations. The State of Utah supported the project through its Economic Development Board, and the University of Utah through the Office of the Vice President for Research. The experimental site became available through the cooperation of the Utah School and Institutional Trust Lands Administration (SITLA), U.S. Bureau of Land Management (BLM), and the U.S. Air Force. We appreciate the assistance of the State of Utah and Fillmore offices of the BLM in crafting the Plan of Development for the site. We thank Patrick A. Shea who assisted the collaboration with much valuable advice and provided

We are unsure whether the detected downward TGF is a single-pulse or a multi-pulse TGF, as it was detected at the edge of the surface detector. Furthermore, the peak current estimated here is −18 kA, indicating a relatively low-peak current return stroke producing a lightning flash. High-peak current return strokes may exhibit different behaviors in time scales or in optical emissions associated with different chemical components. Consequently, further observations are necessary to understand better the durations of ionic and neutral emissions associated with TGFs.

We are expanding this research to include more TGF observations, focusing on events with multiple bursts and enhancing our optical emission understanding and capabilities with additional instruments, such as a photometric array.

Data Availability Statement

The spectroscopic data (processed data and source python scripts used for figure generation) presented in this article are available through (Kieu et al., 2024).

References

Abbasi, R., Abe, M., Abu-Zayyad, T., Allen, M., Anderson, R., Azuma, R., et al. (2017). The bursts of high energy events observed by the telescope array surface detector. *Physics Letters A*, *381*(32), 2565–2572. https://doi.org/10.1016/j.physleta.2017.06.022

Abbasi, R., Abu-Zayyad, T., Allen, M., Barcikowski, E., Belz, J., Bergman, D., et al. (2018). Gamma ray showers observed at ground level in coincidence with downward lightning leaders. *Journal of Geophysical Research: Atmospheres*, *123*(13), 6864–6879. https://doi.org/10.1029/2017jd027931

Abbasi, R., Saba, M., Belz, J., Krehbiel, P., Rison, W., Kieu, N., et al. (2023). First high-speed video camera observations of a lightning flash associated with a downward terrestrial gamma-ray flash. *Geophysical Research Letters*, *50*(14), e2023GL102958. https://doi.org/10.1029/2023gl102958

Abu-Zayyad, T., Aida, R., Allen, M., Anderson, R., Azuma, R., Barcikowski, E., et al. (2012). The surface detector array of the telescope array experiment. *Nuclear Instruments and Methods in Physics Research Section A: Accelerators, Spectrometers, Detectors and Associated Equipment*, *689*, 87–97. https://doi.org/10.1016/j.nima.2012.05.079

Babich, L., Bochkov, E., Kutsyk, I., Neubert, T., & Chanrion, O. (2015). A model for electric field enhancement in lightning leader tips to levels allowing x-ray and \gamma ray emissions. *Journal of Geophysical Research: Space Physics*, *120*(6), 5087–5100. https://doi.org/10.1002/2014ja020923

Babich, L. P. (2005). Analysis of a new electron-runaway mechanism and record-high runaway-electron currents achieved in dense-gas discharges. *Physics-Uspekhi*, *48*(10), 1015–1037. https://doi.org/10.1070/pu2005v048n10abeh002805

Belz, J., Krehbiel, P., Remington, J., Stanley, M., Abbasi, R., LeVon, R., et al. (2020). Observations of the origin of downward terrestrial gamma-ray flashes. *Journal of Geophysical Research: Atmospheres*, *125*(23), e2019JD031940. https://doi.org/10.1029/2019jd031940

Bjørge-Engeland, I., Østgaard, N., Mezentsev, A., Skeie, C. A., Sarria, D., Lapierre, J., et al. (2022). Terrestrial gamma-ray flashes with accompanying elves detected by asim. *Journal of Geophysical Research: Atmospheres*, *127*(11), e2021JD036368. https://doi.org/10.1029/2021jd036368

Briggs, M., Fishman, G., Connaughton, V., Bhat, P., Paciesas, W., Preece, R., et al. (2010). First results on terrestrial gamma ray flashes from the fermi gamma-ray burst monitor. *Journal of Geophysical Research*, *115*(A7). https://doi.org/10.1029/2009ja015242

Briggs, M. S., Xiong, S., Connaughton, V., Tierney, D., Fitzpatrick, G., Foley, S., et al. (2013). Terrestrial gamma-ray flashes in the fermi era: Improved observations and analysis methods. *Journal of Geophysical Research: Space Physics*, *118*(6), 3805–3830. https://doi.org/10.1002/jgra.50205

Carlson, B., Lehtinen, N. G., & Inan, U. S. (2007). Constraints on terrestrial gamma ray flash production from satellite observation. *Geophysical Research Letters*, *34*(8). https://doi.org/10.1029/2006gl029229

Carlson, B., Lehtinen, N. G., & Inan, U. S. (2009). Terrestrial gamma ray flash production by lightning current pulses. *Journal of Geophysical Research*, *114*(A12). https://doi.org/10.1029/2009ja014531

Celestin, S., Xu, W., & Pasko, V. (2012). Terrestrial gamma ray flashes with energies up to 100 mev produced by nonequilibrium acceleration of electrons in lightning. *Journal of Geophysical Research*, *117*(A5). https://doi.org/10.1029/2012ja017535

Cen, J., Yuan, P., Xue, S., & Wang, X. (2015). Spectral characteristics of lightning dart leader propagating in long path. *Atmospheric Research*, *164*, 95–98. https://doi.org/10.1016/j.atmosres.2015.04.019

Chaffin, J. M., Smith, D. M., Lapierre, J., Cummer, S., Ortberg, J., Sunjerga, A., et al. (2024). Mountaintop gamma ray observations of three terrestrial gamma-ray flashes at the säntis tower, Switzerland with coincident radio waveforms. *Journal of Geophysical Research: Atmospheres*, *129*(2), e2023JD039761. https://doi.org/10.1029/2023jd039761

Dwyer, J. (2003). A fundamental limit on electric fields in air. *Geophysical Research Letters*, *30*(20). https://doi.org/10.1029/2003gl017781

Dwyer, J., Rassoul, H., Al-Dayeh, M., Caraway, L., Wright, B., Chrest, A., et al. (2004). A ground level gamma-ray burst observed in association with rocket-triggered lightning. *Geophysical Research Letters*, *31*(5). https://doi.org/10.1029/2003gl018771

Dwyer, J., Schaal, M., Cramer, E., Arabshahi, S., Liu, N., Rassoul, H., et al. (2012). Observation of a gamma-ray flash at ground level in association with a cloud-to-ground lightning return stroke. *Journal of Geophysical Research*, *117*(A10). https://doi.org/10.1029/2012ja017810

Dwyer, J. R. (2005). The initiation of lightning by runaway air breakdown. *Geophysical Research Letters*, *32*(20). https://doi.org/10.1029/2005gl023975

Dwyer, J. R. (2007). Relativistic breakdown in planetary atmospheres. *Physics of Plasmas*, *14*(4). https://doi.org/10.1063/1.2709652

Dwyer, J. R. (2008). Source mechanisms of terrestrial gamma-ray flashes. *Journal of Geophysical Research*, *113*(D10). https://doi.org/10.1029/2007jd009248

Dwyer, J. R. (2012). The relativistic feedback discharge model of terrestrial gamma ray flashes. *Journal of Geophysical Research*, *117*(A2). https://doi.org/10.1029/2011ja017160

support for the collaboration's efforts. The people and the officials of Millard County, Utah have been a source of steadfast and warm support for our work which we greatly appreciate. We are indebted to the Millard County Road Department for their efforts to maintain and clear the roads which get us to our sites. We gratefully acknowledge the contribution from the technical staffs of our home institutions. An allocation of computing resources from the Center for High Performance Computing at the University of Utah as well as the Academia Sinica Grid Computing Center (ASGC) is gratefully acknowledged. We thank Ryan Said and W. A. Brooks of Vaisala Inc. for providing quality NLDN data lightning discharges over and around the TASD under their academic research use policy. F.J.G.V. acknowledges the financial support from the Spanish Ministry of Science and Innovation, MCIN, under project PID2022-136348NB-C31, FEDER program, and under the research grant CEX2021-001131-S funded by MCIN/AEI/10.13039/501100011033.

Dwyer, J. R., & Cummer, S. A. (2013). Radio emissions from terrestrial gamma-ray flashes. *Journal of Geophysical Research: Space Physics*, *118*(6), 3769–3790. https://doi.org/10.1002/jgra.50188

Dwyer, J. R., & Smith, D. M. (2005). A comparison between Monte Carlo simulations of runaway breakdown and terrestrial gamma-ray flash observations. *Geophysical Research Letters*, *32*(22). https://doi.org/10.1029/2005gl023848

Fishman, G. J., Bhat, P., Mallozzi, R., Horack, J., Koshut, T., Kouveliotou, C., et al. (1994). Discovery of intense gamma-ray flashes of atmospheric origin. *Science*, *264*(5163), 1313–1316. https://doi.org/10.1126/science.264.5163.1313

Gjesteland, T., Østgaard, N., Collier, A., Carlson, B., Eyles, C., & Smith, D. (2012). A new method reveals more tgfs in the rhessi data. *Geophysical Research Letters*, *39*(5). https://doi.org/10.1029/2012gl050899

Gjesteland, T., Østgaard, N., Connell, P., Stadsnes, J., & Fishman, G. (2010). Effects of dead time losses on terrestrial gamma ray flash measurements with the burst and transient source experiment. *Journal of Geophysical Research*, *115*(A5). https://doi.org/10.1029/2009ja014578

Grefenstette, B. W., Smith, D. M., Hazelton, B., & Lopez, L. (2009). First rhessi terrestrial gamma ray flash catalog. *Journal of Geophysical Research*, *114*(A2). https://doi.org/10.1029/2008ja013721

Gurevich, A., Milikh, G., & Roussel-Dupre, R. (1992). Runaway electron mechanism of air breakdown and preconditioning during a thunderstorm. *Physics Letters A*, *165*(5–6), 463–468. https://doi.org/10.1016/0375-9601(92)90348-p

Gurevich, A., Zybin, K., & Medvedev, Y. V. (2007). Runaway breakdown in strong electric field as a source of terrestrial gamma flashes and gamma bursts in lightning leader steps. *Physics Letters A*, *361*(1–2), 119–125. https://doi.org/10.1016/j.physleta.2006.05.063

Gurevich, A. V., & Zybin, K. P. (2001). Runaway breakdown and electric discharges in thunderstorms. *Physics-Uspekhi*, *44*(11), 1119–1140. https://doi.org/10.1070/pu2001v044n11abeh000939

Hare, B., Uman, M., Dwyer, J., Jordan, D., Biggerstaff, M., Caicedo, J., et al. (2016). Ground-level observation of a terrestrial gamma ray flash initiated by a triggered lightning. *Journal of Geophysical Research: Atmospheres*, *121*(11), 6511–6533. https://doi.org/10.1002/2015jd024426

Harley, J., Zimmerman, L. A., Edens, H. E., Stenbaek-Nielsen, H. C., Haaland, R. K., Sonnenfeld, R. G., & McHarg, M. G. (2021). High-speed spectra of a bolt from the blue lightning stepped leader. *Journal of Geophysical Research: Atmospheres*, *126*(3), e2020JD033884. https://doi.org/10.1029/2020jd033884

Heumesser, M., Chanrion, O., Neubert, T., Christian, H. J., Dimitriadou, K., Gordillo-Vazquez, F. J., et al. (2021). Spectral observations of optical emissions associated with terrestrial gamma-ray flashes. *Geophysical Research Letters*, *48*(4), 2020GL090700. https://doi.org/10.1029/2020gl090700

Kieu, et al. (2024). Data submissions for the first time-resolved leader spectra associated with downward terrestrial gamma ray flash detected at the telescope array surface detectors. Retrieved from https://osf.io/m2yxw/?view_only=c96860d3663d4daf8c080bc8a0f8d0bb

Kieu, N., Gordillo-Vázquez, F., Passas, M., Sánchez, J., Pérez-Invernón, F. J., Luque, A., et al. (2020). Submicrosecond spectroscopy of lightning-like discharges: Exploring new time regimes. *Geophysical Research Letters*, *47*(15), e2020GL088755. https://doi.org/10.1029/2020gl088755

Kieu, N., Gordillo-Vázquez, F. J., Passas, M., Sánchez, J., & Pérez-Invernón, F. J. (2021). High-speed spectroscopy of lightning-like discharges: Evidence of molecular optical emissions. *Journal of Geophysical Research: Atmospheres*, *126*(11), e2021JD035016. https://doi.org/10.1029/2021jd035016

Köhn, C., Chanrion, O., Nishikawa, K., Babich, L., & Neubert, T. (2020a). The emission of energetic electrons from the complex streamer corona adjacent to leader stepping. *Plasma Sources Science and Technology*, *29*(3), 035023. https://doi.org/10.1088/1361-6595/ab6e57

Köhn, C., Diniz, G., & Harakeh, M. N. (2017). Production mechanisms of leptons, photons, and hadrons and their possible feedback close to lightning leaders. *Journal of Geophysical Research: Atmospheres*, *122*(2), 1365–1383. https://doi.org/10.1002/2016jd025445

Köhn, C., & Ebert, U. (2015). Calculation of beams of positrons, neutrons, and protons associated with terrestrial gamma ray flashes. *Journal of Geophysical Research: Atmospheres*, *120*(4), 1620–1635. https://doi.org/10.1002/2014jd022229

Köhn, C., Heumesser, M., Chanrion, O., Nishikawa, K., Reglero, V., & Neubert, T. (2020b). The emission of terrestrial gamma ray flashes from encountering streamer coronae associated to the breakdown of lightning leaders. *Geophysical Research Letters*, *47*(20), e2020GL089749. https://doi.org/10.1029/2020gl089749

Köhn, C., Heumesser, M., Chanrion, O., Reglero, V., Østgaard, N., Christian, H. J., et al. (2024). Employing optical lightning data to identify lightning flashes associated to terrestrial gamma-ray flashes. *Bulletin of Atmospheric Science and Technology*, *5*(1), 2. https://doi.org/10.1007/s42865-024-00065-y

Kramida, A., Ralchenko, Y., Reader, J., Team, N. A., et al. (2012). National institute of standards and technology.

Lindanger, A., Skeie, C. A., Marisaldi, M., Bjørge-Engeland, I., Østgaard, N., Mezentsev, A., et al. (2022). Production of terrestrial gamma-ray flashes during the early stages of lightning flashes. *Journal of Geophysical Research: Atmospheres*, *127*(8), e2021JD036305. https://doi.org/10.1029/2021jd036305

Liu, N., Dwyer, J. R., Tilles, J. N., Stanley, M. A., Krehbiel, P. R., Rison, W., et al. (2019). Understanding the radio spectrum of thunderstorm narrow bipolar events. *Journal of Geophysical Research: Atmospheres*, *124*(17–18), 10134–10153. https://doi.org/10.1029/2019jd030439

Marisaldi, M., Argan, A., Trois, A., Giuliani, A., Tavani, M., Labanti, C., et al. (2010). Gamma-ray localization of terrestrial gamma-ray flashes. *Physical Review Letters*, *105*(12), 128501. https://doi.org/10.1103/physrevlett.105.128501

Marisaldi, M., Fuschino, F., Labanti, C., Galli, M., Longo, F., Del Monte, E., et al. (2010). Detection of terrestrial gamma ray flashes up to 40 mev by the agile satellite. *Journal of Geophysical Research*, *115*(A3). https://doi.org/10.1029/2009ja014502

Neubert, T., Østgaard, N., Reglero, V., Chanrion, O., Heumesser, M., Dimitriadou, K., et al. (2020). A terrestrial gamma-ray flash and ionospheric ultraviolet emissions powered by lightning. *Science*, *367*(6474), 183–186. https://doi.org/10.1126/science.aax3872

Ortberg, J., Smith, D. M., Li, J., Dwyer, J., & Bowers, G. (2020). Detecting an upward terrestrial gamma ray flash from its reverse positron beam. *Journal of Geophysical Research: Atmospheres*, *125*(6), e2019JD030942. https://doi.org/10.1029/2019jd030942

Orville, R. E. (1968). Spectrum of the lightning stepped leader. *Journal of Geophysical Research*, *73*(22), 6999–7008. https://doi.org/10.1029/jb073i022p06999

Orville, R. E. (1975). Spectrum of the lightning dart leader. *Journal of the Atmospheric Sciences*, *32*(9), 1829–1837. https://doi.org/10.1175/1520-0469(1975)032<1829:sotldl>2.0.co;2

Østgaard, N., Cummer, S. A., Mezentsev, A., Luque, A., Dwyer, J., Neubert, T., et al. (2021). Simultaneous observations of eip, tgf, elve, and optical lightning. *Journal of Geophysical Research: Atmospheres*, *126*(11), e2020JD033921. https://doi.org/10.1029/2020jd033921

Østgaard, N., Gjesteland, T., Carlson, B., Collier, A., Cummer, S., Lu, G., & Christian, H. (2013). Simultaneous observations of optical lightning and terrestrial gamma ray flash from space. *Geophysical Research Letters*, *40*(10), 2423–2426. https://doi.org/10.1002/grl.50466

Østgaard, N., Neubert, T., Reglero, V., Ullaland, K., Yang, S., Genov, G., et al. (2019). First 10 months of tgf observations by asim. *Journal of Geophysical Research: Atmospheres*, *124*(24), 14024–14036. https://doi.org/10.1029/2019jd031214

Rison, W., Thomas, R. J., Krehbiel, P. R., Hamlin, T., & Harlin, J. (1999). A gps-based three-dimensional lightning mapping system: Initial observations in central New Mexico. *Geophysical Research Letters*, *26*(23), 3573–3576. https://doi.org/10.1029/1999gl010856

Skeie, C., Østgaard, N., Mezentsev, A., Bjørge-Engeland, I., Marisaldi, M., Lehtinen, N., et al. (2022). The temporal relationship between terrestrial gamma-ray flashes and associated optical pulses from lightning. *Journal of Geophysical Research: Atmospheres*, *127*(17), e2022JD037128. https://doi.org/10.1029/2022jd037128

Smith, D. M., Lopez, L. I., Lin, R. P., & Barrington-Leigh, C. P. (2005). Terrestrial gamma-ray flashes observed up to 20 mev. *Science*, *307*(5712), 1085–1088. https://doi.org/10.1126/science.1107466

Stock, M., Akita, M., Krehbiel, P., Rison, W., Edens, H., Kawasaki, Z., & Stanley, M. (2014). Continuous broadband digital interferometry of lightning using a generalized cross-correlation algorithm. *Journal of Geophysical Research: Atmospheres*, *119*(6), 3134–3165. https://doi.org/10.1002/2013jd020217

Tavani, M., Marisaldi, M., Labanti, C., Fuschino, F., Argan, A., Trois, A., et al. (2011). Terrestrial gamma-ray flashes as powerful particle accelerators. *Physical Review Letters*, *106*(1), 018501. https://doi.org/10.1103/physrevlett.106.018501

Thomas, R. J., Krehbiel, P. R., Rison, W., Hunyady, S. J., Winn, W. P., Hamlin, T., & Harlin, J. (2004). Accuracy of the lightning mapping array. *Journal of Geophysical Research*, *109*(D14). https://doi.org/10.1029/2004jd004549

Tran, M., Rakov, V., Mallick, S., Dwyer, J., Nag, A., & Heckman, S. (2015). A terrestrial gamma-ray flash recorded at the lightning observatory in gainesville, Florida. *Journal of Atmospheric and Solar-Terrestrial Physics*, *136*, 86–93. https://doi.org/10.1016/j.jastp.2015.10.010

Wada, Y., Enoto, T., Nakamura, Y., Morimoto, T., Sato, M., Ushio, T., et al. (2020). High peak-current lightning discharges associated with downward terrestrial gamma-ray flashes. *Journal of Geophysical Research: Atmospheres*, *125*(4), e2019JD031730. https://doi.org/10.1029/2019jd031730

Wada, Y., Morimoto, T., Nakamura, Y., Wu, T., Enoto, T., Nakazawa, K., et al. (2022). Characteristics of low-frequency pulses associated with downward terrestrial gamma-ray flashes. *Geophysical Research Letters*, *49*(5), e2021GL097348. https://doi.org/10.1029/2021gl097348

Walker, T. D., & Christian, H. J. (2017). Triggered lightning spectroscopy: Part 1. A qualitative analysis. *Journal of Geophysical Research: Atmospheres*, *122*(15), 8000–8011. https://doi.org/10.1002/2016jd026419

Walker, T. D., & Christian, H. J. (2019). Triggered lightning spectroscopy: 2. A quantitative analysis. *Journal of Geophysical Research: Atmospheres*, *124*(7), 3930–3942. https://doi.org/10.1029/2018jd029901

Warner, T. A., Orville, R. E., Marshall, J., & Huggins, K. (2011). Spectral (600–1050 nm) time exposures (99.6 \mus) of a lightning stepped leader. *Journal of Geophysical Research*, *116*(D12), D12210. https://doi.org/10.1029/2011jd015663

Xu, W., Celestin, S., & Pasko, V. P. (2012). Source altitudes of terrestrial gamma-ray flashes produced by lightning leaders. *Geophysical Research Letters*, *39*(8). https://doi.org/10.1029/2012gl051351

Xu, W., Celestin, S., & Pasko, V. P. (2015). Optical emissions associated with terrestrial gamma ray flashes. *Journal of Geophysical Research: Space Physics*, *120*(2), 1355–1370. https://doi.org/10.1002/2014ja020425